

TraceNet: Segment one thing efficiently

Mingyuan Wu¹, Zichuan Liu², Haozhen Zheng¹, Hongpeng Guo¹, Bo Chen¹, Xin Lu², Klara Nahrstedt¹

¹University of Illinois at Urbana-Champaign, Urbana, IL, USA

²Independent Researcher, USA

ABSTRACT

Efficient single instance segmentation is essential for unlocking features in the mobile imaging applications, such as capture or editing. Existing on-the-fly mobile imaging applications scope the segmentation task to portraits or the salient subject due to the computational constraints. Instance segmentation, despite its recent developments towards efficient networks, is still heavy due to the cost of computation on the entire image to identify all instances. To address this, we propose and formulate a one tap driven single instance segmentation task that segments a single instance selected by a user via a positive tap. This task, in contrast to the broader task of segmenting anything as suggested in the Segment Anything Model [19], focuses on efficient segmentation of a single instance specified by the user. To solve this problem, we present TraceNet, which explicitly locates the selected instance by way of receptive field tracing. TraceNet identifies image regions that are related to the user tap and heavy computations are only performed on selected regions of the image. Therefore overall computation cost and memory consumption are reduced during inference. We evaluate the performance of TraceNet on instance IoU average over taps and the proportion of the region that a user tap can fall into for a high-quality single-instance mask. Experimental results on MS-COCO and LVIS demonstrate the effectiveness and efficiency of the proposed approach. TraceNet can jointly achieve the efficiency and interactivity, filling in the gap between needs for efficient mobile inference and recent research trend towards multimodal and interactive segmentation models.

1 INTRODUCTION

The development of image segmentation has never been stopped in the past decades due to its critical role in image understanding applications [1, 29, 32?]. The initial goal of image segmentation is to segment out objects of certain semantic categories as defined in the tasks of semantic segmentation and instance segmentation. Most literature under the umbrella of these tasks [10, 13, 16] have been focusing on improving the segmentation accuracy. To further aid segmentation accuracy, user inputs have been considered as additional cues and modalities. In particular, traditional click-based interactive image segmentation optimizes for the minimal number of clicks to achieve a satisfactory segmentation result on user specified objects. Going beyond clicks, latest large promptable segmentation models [19, 51] are designed and trained to take a variety of user queries including boxes, scribbles, masks and free-form texts. These models demonstrate strong zero-shot generalization to new downstream vision tasks and new image distributions. At the same time, these models enable more segmentation pipelines to involve multimodal user inputs, and significantly increase interactivity in the inference stage.

Despite a trend towards multimodal and interactive segmentation, mobile applications, as natural interfaces to obtain user prompts, have not fully enjoyed recent advancement of the segmentation algorithms. A gap exists between the inefficiency and heavy computation of the segmentation algorithms and limited computational resources in mobile scenarios. To bridge the gap, researchers have been investigating efficient approaches for segmentation so that the algorithms can run smoothly in mobile editing apps or even capture apps. Efficient segmentation approaches [3, 4, 6, 20, 41, 44, 45] usually are build upon efficient neural network architectures [7, 15, 38]. In practical cases that require extreme efficiency, mobile applications with these algorithms limit the number of semantic categories, or focus on the salient subject in the scene. A representative successful application of efficient segmentation approaches is the portrait mode that is widely supported in default camera apps on mobile phones¹. This mode employs portrait segmentation techniques, generally limited to binary semantic categories such as person versus background or salient object versus background, to enhance efficiency. As far as we know, the potential for a facilitative relationship between interactivity and efficiency and jointly achieving both of them remains unexplored in segmentation literature and industry applications. In this context of efficient and interactive segmentation for mobile imaging applications, we propose to use user inputs (such as an arbitrary tap on the instance) to enable efficient single-instance segmentation. The proposed formulation relaxes the limitation of existing efficient segmentation that applies only to the salient subject in the scene. As shown in Figure 1(a), with a tap of the dog, unicorn, or pumpkin, we expect to get its segmentation mask instantly. With the tap-based single-instance segmentation, automatic images manipulation, such as depth-of-field effects, background replacement and image enhancement, therefore can be enabled on an arbitrary instance in the image.

That is, we strive for a more specific type of segmentation model for mobile applications and answer a question: **since users have already indicated interactively what object they like on their phones, what should our efficient segmentation model do smartly**. Formally, We propose a novel form of image segmentation task, namely **one tap efficient segmentation**, which is motivated by the demands of on-the-fly image editing mobile applications. The task aims at segmenting one instance that a user queries with a positive tap in an extremely efficient manner. We use "taps" to better represent intuitive user interactions with modern mobile applications, as opposed to "clicks" associated with mouse-driven desktop environments. It is worth mentioning that modern mobile devices register a tap as a specific pixel input, rather than a broader area in the image. In practical scenarios of one-tap efficient segmentation,

¹iphone portrait mode: <https://support.apple.com/en-us/HT208118>, Pixel6 portrait mode: https://store.google.com/us/magazine/pixel_camera?hl=en-US

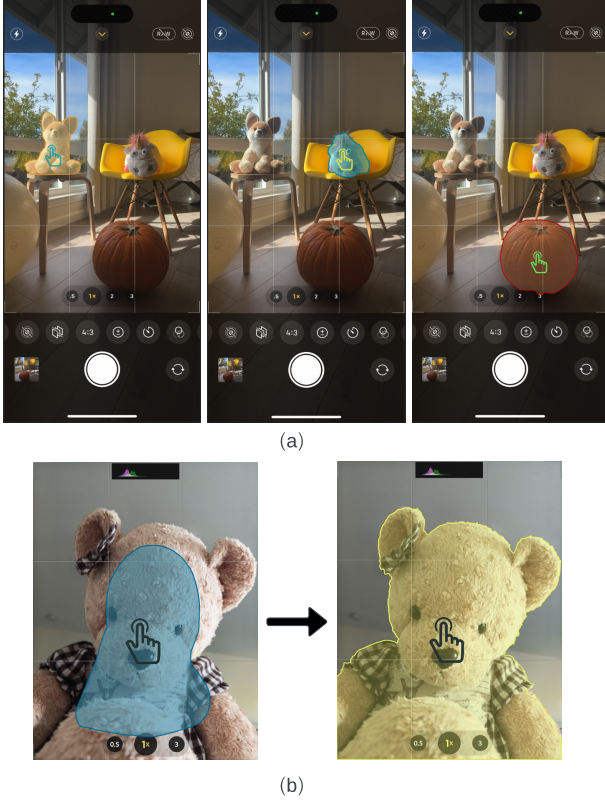


Figure 1: Tap-driven Single-Instance Segmentation: (a) A single instance mask is produced when a user taps an instance in the viewfinder. (b) The clickable region supported by our algorithm is highlighted in blue and the predicted instance mask is highlighted in yellow. Various local adjustments are expected to happen in the yellow area before the image is captured in the mobile applications.

a user's tap might not always accurately target the center of the desired instance. The imperfect click might result in an unsatisfying segmentation result that affects user experience. To improve user experience, we propose a metric of user tap tolerance in addition to segmentation accuracy. This metric measures the proportion of the region that a user tap can fall into for a high-quality single-instance mask, as shown in Figure 1 (b).

Our research insight towards the proposed problem is that the user tap could serve as a cue to guide the model to perform inference in a selective manner. Following the insight, we propose a straightforward yet effective solution **TraceNet**, which employs **receptive field tracing** through the neural network to explicitly locate the selected instance, thereby avoiding the need for intensive feature computation across the entire image. TraceNet is inspired by recently proposed conditional instance segmentation methods [41, 48], which predicts local query features around the single instance and dynamically conditions the instance-aware mask head on the local features. Based on the conditional mechanism, TraceNet can dynamically control inference given a tap query. Since local relevant features around the user tap of the instance are important to guide the segmentation prediction, a receptive-field tracer (RFT) is introduced to control the spatial region where heavy computation

is applied to. The controller back-traces computation dependency across each layer and crops out all pixels that do not contribute to the local features around the tap. The cropping is conducted in the forwarding pass, eliminating spatially redundant convolution operations. Overall our contribution can be summarized as follows:

- Motivated by real-world demands, we proposed and formulated a **one tap efficient segmentation** as a new form of efficient segmentation for a single instance, and designed evaluation protocols.
- We propose a solution of TraceNet for one tap efficient segmentation. TraceNet conditions the instance-aware mask head on local features around the user's click and efficiently controls the usage of local features.
- We evaluated the proposed TraceNet on MS-COCO [23] and LVIS [12]. TraceNet demonstrates high computational efficiency while achieving high accuracy on the mask prediction of user-specified instances along with a high user tap tolerance.

2 RELATED WORK

The proposed problem of one tap efficient segmentation aligns closely with a broad line of segmentation research that leverages user clicks. We review studies in these categories and discuss differences of our target. Meanwhile, as one tap segmentation can be achieved by performing segmentation of all instances, we review studies that directly predict dense instance masks and discuss the efficiency advantage of the proposed method. Lastly, the proposed TraceNet efficiently makes use of relevant image features with regard to the user tap, which is related to studies that aim to avoid applying heavy convolutions on the entire images.

2.1 Click-based Interactive Segmentation

Most of existing interactive segmentation pipelines in the literature optimize for the minimal user clicks so that the IoU (Intersection over Union) between the predicted foreground mask and the groundtruth mask exceeds a pre-defined threshold. Classic methods in this field typically utilize low-level image features and the properties of clicks. Well-known traditional approaches include Intelligent Scissors [33, 34], Graphcut [5], Grabcut [37], and Random-walk [11]. The advent of CNN-based interactive segmentation was marked by the introduction of DIOS [46]. This method translates user clicks into Euclidean distance maps, which are then merged with the original RGB channels for input into a fully convolutional network [30]. In recent years, the paradigm of clicks encoding and concatenation are widely followed by further works in various learning-based interactive segmentation schemes [9, 18, 25, 26, 28, 39, 40, 50]. In addition to these specialized interactive segmentation models, vision foundation models have also demonstrated capability in this area. SAM [19], in particular, has attracted significant attention for its remarkable zero-shot generalization to new image distributions and tasks. SAM operates by conditioning its mask decoder on combined output embeddings from a heavy image encoder and a prompt encoder, inherently functioning as an interactive segmenter for any instance. MobileSAM [49] makes SAM more mobile-friendly by distilling the knowledge from SAM's heavy encoder into a more

lightweight one. However, our task differs from conventional interactive segmentation, as it focuses on efficiently segmenting a single instance rather than segmenting anything or everything. Guided by a user’s tap within one instance, TraceNet can selectively encode the instance-relevant features and thus benefit from efficiency gains as it avoids redundant all-instance aware feature calculation across the entire image.

2.2 Image-level Mask Predictions

Recent efficient instance segmentation approaches take the entire image as input and predict dense instance masks directly [3, 41, 48]. Unlike Mask-RCNN [13], these approaches avoid ROI operations to obtain local feature maps and are more efficient as a result. YOLACT+ [3] breaks the segmentation task into generating prototype masks and directly predicting per-instance mask coefficients. Condinst[41] adds a dynamic instance-aware mask branch to the object detector FCOS[42]. With parameters conditioned on local features individual instance, the mask branch can be directly applied to predict instance masks from the whole feature map . SOIT[48] is a follow-up conditional image-level prediction algorithm that applies encoder-decoder transformer architecture to produce instance-related query features. While these image-level prediction algorithms generally achieve a much faster inference speed, there is room for efficiency improvement, especially only one specific instance mask is queried by users. TraceNet addresses this gap, offering a principled approach to enhance the efficiency of these models in one-instance cases.

2.3 Spatial Redundancy of Convolution

In most of the convolutional neural networks, convolution is the most computational heavy operator that impacts inference time. Reducing computation cost by applying convolution on selected areas of images has been successfully pursued. For example, in the task of small/multi-level object detection, AutoFocus[35] targets multi-level efficient inference. It predicts and crop segmentation map at coarser scales, and then runs the detector at finer scales on a small fraction of the entire image. QueryDet[47] predicts the coarse locations of small objects on low-resolution features, and then runs sparse convolution on high-resolution feature spatially guided by the coarser predictions. In AutoFocus and QueryDet, “focus cropping” operations are conducted either on images or feature maps, improving inference speed of (small) object detection. The gain of inference speed is led by the sparsity of small objects.

3 TASK AND METHOD

Problem Formulation. Given an input image $I \in \mathbb{R}^{H \times W \times 3}$ and a user tap $c = (x, y) \in \mathbb{R}^{H \times W}$. The goal of tap-driven single-instance segmentation is to predict a pixel-level mask of the instance located at (x, y) . The ground-truth is defined by $\{M_{gt}\}$, where $M_{gt} \in \{0, 1\}^{H \times W}$ is the groundtruth mask that user queries with the tap c , where $c \in M_{gt}$. The expected model is a learned function that maps I and c to a single-instance mask M_{pred} , targeting a satisfying IoU between M_{pred} and M_{gt} . Because M_{pred} depends on the user tap c , we propose a new metric, the mean tap Intersection over Union (mIoU-T), to measure the average segmentation accuracy of

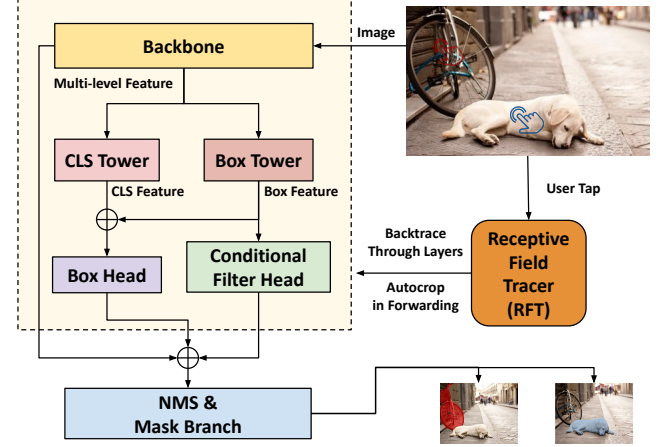


Figure 2: - The overall architecture of TraceNet. Based on a User Tap, Receptive Field Tracer back traces the receptive field region and perform autocropping in all convolution heads except the mask branch. Details of receptive field backtracing, autocropping and other modules for instance segmentation are discussed in section 3.

all possible user taps within the groundtruth instance mask. The user tap tolerance is measured by the newly proposed metric mean Tap Area (mTA). mTA calculates the ratio between area of feasible taping area and the area of groundtruth instance mask. The feasible taping area covers potential taps that can generate an instance mask with the IoU over a predefined threshold. We refer readers to the experiment section 4.2 for the formula of mIoU-T and mTA.

Overall System Architecture. As shown in Figure 2, TraceNet introduces a key component named Receptive Field Tracer (RFT). The Receptive Field Tracer targets eliminating the computation redundancy in the exhausted searching for instances in existing instance segmentation algorithms towards tap-driven segmentation. Given a user tap, the RFT back-traces the receptive field region at each layer with respect to local features around the user query tap. The receptive field back-tracing can be regarded as a Depth-First Search process that recursively computes receptive fields from downstream layers to upper-stream layers. Based on the derived receptive fields, the features that do not contribute to the output related to the user tap will be removed during the inference phase. Thus, RFT reduces the computation by controlling the inference flow of the most parts of an instance segmentation model. During the inference phase, the RFT removes the redundant computation that does not contribute to the output, which brings significant performance improvement in running speed and memory consumption. The RFT can be applied to convolutional instance segmentation algorithms in general.

3.1 Receptive Field Back-Tracing in TraceNet

As it is shown in Figure 3, receptive field of each layer in the computation graph of instance segmentation is backtraced recursively, enabling autocropping function in the forwarding pass and saving computations. Details will be discussed in this section. The section is organized as follows: we will first give a formal definition of receptive field region at each layer in neural networks, then give a detail post-order Depth First Search algorithm illustrating the

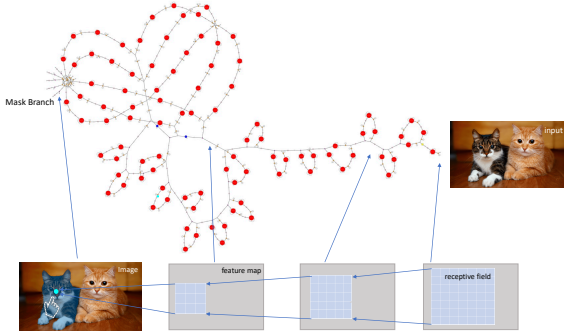


Figure 3: One tap driven receptive field back tracing in the acyclic computation graph (visualized directly by onnx) of instance segmentation. The receptive field is backtraced recursively with post-order Depth-first search. Computations in grey regions are significantly reduced with autocropping mechanism

mechanism of receptive field back-tracing in arbitrary pure convolution neural network models, derive all the recursive cases and finally explain how Receptive Field Tracer makes use of the results to control the calculation of other components during the inference process.

Receptive Field Revisited. In the context of deep learning[2, 31], *receptive field region* refers to the region in the input that produces the feature. *Receptive field* is defined as the size of the region. The concept of receptive field is important for researchers to diagnose how CNN works in a sense that a unit in the model output is only affected by units in receptive field regions in the input image. A formal definition of the receptive field region of a simple n -layer convolutional neural network can be formulated as follows. Assume the pixels on each layer are indexed by (i, j) , with the most upper-left pixel at $(0, 0)$. Denote the (i, j) th pixel on the p th layer as $x_{i,j}^p$, $p \in [n]$ in a n -layer convolutional neural network where $x_{i,j}^0$ and $x_{i,j}^n$ respectively denote the pixel value in the input image and the model output. By definition the receptive field region of the unit $x_{i,j}^n$ is the set of all units in x^0 that contribute to $x_{i,j}^n$. The receptive field region of a set of units is the union of the receptive field region of all units in the set. We extend the concept of the receptive field more than in the input images and define *the p -layer receptive field region* r^p of the unit $x_{i,j}^n$ to be the set of all units in the output feature map of the p th layer x^p that contribute to $x_{i,j}^n$ for any $p \in [n]$. Note that we can consider only single channel of the input and output of each layer in the context of calculating receptive field regions and similar results can be derived for layers with multiple channels.

Receptive Field Depth First Search. The tap-driven segmentation aims at precisely localizing the region that contributes to local output features around user taps and reducing spatial redundancy of convolution operations as much as possible across all the layers of the model. i.e only computation within the layer receptive field region is preserved in forward pass. We introduce a tap-driven receptive field back-tracing algorithm to compute receptive field regions at each layer of the neural network from deep to shallow.

To illustrate the algorithm, we construct a directed acyclic computation graph for arbitrary model, where the nodes correspond to layer operations and inputs, and directed edges represent dependency between layers. (Note that most modern convolutional neural networks designs [14][21] rely on layers with multiple child nodes and more than one back-tracing paths exist.) To deal with arbitrary neural network model, the calculation of receptive field region at each layer is conducted in post-order Depth First Search with an intuition that p -layer receptive field region can be represented as a function of receptive field regions of all the child nodes of the p -layer node. In post-order Depth First Search, the receptive field region of the p -layer will be calculated after all the child nodes of the p -layer have been visited. The search algorithm ensures single visit of each node and results in a worst-case complexity of $O(|\mathcal{E}| + |\mathcal{N}|)$, where \mathcal{E} represents the edge set and \mathcal{N} represents the node set in the computation graph of the model.

Recursive Case Setup: from $p+1$ to p . For simplicity of notation, we first describe the problem setup of receptive field region calculation in computation graph with only one path including all nodes. The setup can be naturally extended to arbitrary computational graph with the Depth First Search solution. Consider a pure convolutional neural network model with P layer operations and the layer index $p \in [P]$. i.e, for any $p \in [P - 1]$, the node representing the p th layer in the computation graph has one and only one child node representing the $(p + 1)$ th layer. The layer operation $type(p)$ can be one of the common operations in Neural Network including *Convolution, Activation, Pooling, Normalization, Interpolation*. Define the feature map f_p as the output feature map of the p th layer. For any $p \in [P - 1]$, We want to derive a recursive and invertible mapping function that maps r^{p+1} with respect to f_{p+1} to r^p with respect to f_p , based on the type of the layer $(p + 1)$ and a list of parameters A_{p+1} that characterize the layer $(p + 1)$.

$$r^p = F(r^{p+1}, A_{p+1}) \quad (1)$$

Recursive Case of Convolution. Under the single channel assumption mentioned in previous section, 4 common parameters are left for the spatial configuration of the p th convolutional layer. Denote the kernel size as k_p , stride as s_p , padding as q_p , dilation factor as α . i.e $A_p = [k_p, s_p, q_p, \alpha]$. The function F is deterministic and unique, given the same state of the convolution operations. One representation of the recursive mapping function F in 1-D dimension is given in [2]. For 2D images, the derivations can be applied to both dimensions independently because the receptive field region is rectangular in the simplified problem setup. Denote u_p and v_p as the left-most and right-most zero-indexed coordinates of r_p with respect to f_p .

$$u_p = -q_{p+1} + u_{p+1} \cdot s_{p+1} \quad (2)$$

$$v_p = -q_{p+1} + v_{p+1} \cdot s_{p+1} + \alpha(k_{p+1} - 1) \quad (3)$$

F is defined to map 1-D interval $[u_{p+1}, v_{p+1}]$ to $[u_p, v_p]$. Note that the receptive field region can possibly exceed the boarder of the feature map because of non-zero padding. In this case, the controller should memorize how much it exceeds the boarder for a future Autopadding operation in the forwarding pass and set $u_p = \max(u_p, 0)$ and $v_p = \min(v_p, width)$. The same operation is applied to two dimensions of images independently.

Recursive Case of Normalization. Batch normalization[17] exists in many segmentation algorithms, as a widely-used and effective normalization method. Batch normalization makes training of convolutional neural network more stable through normalization along the batch dimension. The batch normalization does not alter the receptive field region in forwarding pass, which means the mapping function F to be an identity function.

Recursive Case of Pooling and Interpolation. A pooling layer a fundamental building block of a convolutional neural network, calculating value for patches of a feature map. The pooling layer downsamples the feature map and results in a larger receptive field. For receptive region computation purpose, pooling by a factor of x is equivalent to a convolutional layer with kernel size and stride x . In contrast, upsampling is often done by interpolation layer such as nearest neighbour, bilinear, bicubic and trilinear. Any pixel in the output feature map of the interpolation layer depends locally on input features. For receptive region computation purpose, the interpolation layer is equivalent to a convolutional layer that has a kernel size equal to the number of input features involved in the computation of an output feature.

Extended Setup for Arbitrary Computation Graph. Suppose the p -layer has m children denoted as p^l such that $l \in [m]$. Denote the receptive field region r^p with respect to the p th layer output f_p ,

$$r^p = \bigcup_{l \in [m]} F(r^{p^l}, A_{p^l}) \quad (4)$$

where F denotes the recursive and invertible mapping function that maps receptive field region of child nodes to the receptive field region with respect to current feature map, based on the type of the child layer operation. Note that the union of the outputs of multiple mapping function F might be the union of more than one rectangular regions. In our PyTorch implementation, we approximate the receptive field region r_p by the smallest rectangular region that fully covers all the back-traced rectangular regions before we further compute the receptive field region at a higher nodes. Note that the smallest rectangular region can be trivially computed by simply comparing the coordinate values of sides of all rectangular receptive field regions. The design choice is based on two practical reasons. 1) Multiple back-traced rectangular regions are often greatly overlapped with each other. Thus, negligible theoretical computation overheads are introduced by computing features in the approximated receptive field region; 2) Pytorch implementations are much more efficient in computing features in a rectangular patch. At each layer, exact input and output of individual F function are memorized by the receptive field region controller for AutoCropping in the forwarding pass.

AutoCropping and AutoPadding. After (approximate) layer receptive field regions have been computed from leaf to root in the computation graph, we can compute features within the approximate receptive field regions from root to leaf. For any p layer and any child node p^l of the p layer, the receptive field region controller crops the feature map with the memorized output of the F function and pads it with the memorized padding value at four boarders for next-layer feature computation in p^l . Any feature value that is

outside the approximate layer receptive field r^p does not contribute to final-layer features around the user click.

3.2 System Implementation Details

This section covers details of TraceNet system implementation besides the RFT module. Note that the RFT module introduced above can be applied to convolutional instance segmentation algorithms in general, with "plug-in" property to reduce computations and memory consumption.

Overall Design Choice. In addition to RFT, as shown in Figure 2, TraceNet includes a feature pyramid backbone[21] that extracts multi-level feature maps from the input image, a conditional filter head that predicts the parameters of the mask head with local features around the tap, a compact mask head conditioned on the user-specified instance in their filters. These components exist in different formats in most of the instance segmentation algorithm paradigms that first attend to all the instances exhaustedly in the image (step I) and then predict the pixel-level masks of the instance (step II). (i.e instance first). Being universal to all of the instance segmentation methods, the RFT can significantly prevent exhausted computation over all the feature maps in step I by Receptive Field Region Tracing mechanism, but cannot save computation in step II, as it is shown in Figure 2. Note that conditional based methods like Condinst [41] is different from and ROI operation based methods like Mask-RCNN [13] in the sense that conditional based methods has heavy computation in step I and a compact mask head in step II, while step II is much heavier in ROI-operation based method. Thus by intuition, the RFT with conditional based methods can result in more significant savings in conditional based methods and less computation overheads left.

Backbone Module. Following the design of Feature Pyramid Network [21], we extract a 5-level feature pyramid over Resnet[14]. Each level of our feature pyramid is used to extract local features around the tap at different scales. The feature pyramid design is essential because no scaling information of the user-specified instance is provided.

Mask Branch Conditioned on Instance. We follow the design of mask branch in Condinst [41]. The mask branch is in the format of Fully Convolutional Neural Network [30] for an image-level prediction. The mask branch is applied to a feature map extracted from the backbone. (i.e P_3 with downsampling ratio of 8). Compared to the mask branch design in Mask RCNN [13], the design eliminates needs for ROI operations by performing convolution in image-level. Besides, the computation overhead of the mask head in our model is much more lightweight. It only consists of 3 1x1 convolution layers with 8 channels each, while the unconditioned mask branch in Mask-RCNN often has four convolution layers with 256 channels. The intuition behind the compact design can be explained as follows. When the parameters of mask branch in our model are conditioned on local features around user-specified instance, the characteristics (geometry of the instance and relative location of the instance with respect to the user query tap) of the user specified instance can be encoded in the mask branch with the help of conditional filter head. To fully exploit the encoded spatial characteristic, we concatenate the P_3 feature map with a map of relative coordinates

from all locations to the user tap query. Similar designs also exist in other conditional instance segmentation algorithms [41, 48]. When applied to the concatenated inputs, the mask branch can naturally focus on the pixels of the user specified instance and predict the mask in an instance-aware manner. A sigmoid is applied to make the mask prediction class-agnostic. Finally, a bilinear 4x upsampling is performed on the output mask. The upsampling results in 2x downsampling mask prediction compared to the resolution of the input image.

Conditional Filter Head and Box Head. The conditional filter head is adopted with slight modification from Condinst[41], which is based on FCOS[42]. In FCOS and Condinst, each pixel location on multi-level feature map can be associated with an instance in the original image by a simple mapping, i.e. The pixel (x, y) at the feature map with downsampling ratio of s can be mapped to the input image as $(\lfloor \frac{s}{2} \rfloor + xs, \lfloor \frac{s}{2} \rfloor + ys)$. Condinst introduces a conditional filter head to encode characteristics of the instance associated with the location in the feature map in pixel-level fashion and a box head to regress the bounding box location of the same instance. The conditional filter head is used to predict a 169-dimension vector of parameters $\theta_{a,b}$ for the above mentioned mask branch for the mask of instance located at (a, b) in the feature map. The box head predicts a 4-dimension vector encoding relative distance between the pixel and four boundaries of the bounding box. Both heads take the features extracted from heavy classification and box tower, which consists of four 3x3 stride 1 convolutional layers with dimension 256 followed by ReLU activation and BN[17]. The centerness head is not included in the Figure 2 and we refer readers to more details in FCOS [42].

Training Target. The loss function adopted is similar to Condinst [43]:

$$L = L_{\text{cls}} + \lambda_1 L_{\text{mask}} + \lambda_2 L_{\text{reg}} \quad (5)$$

It is a balanced loss of classification, bounding box regression and mask prediction. λ_1 and λ_2 are equal to 1 in the experiment. We refer readers for more details of L_{cls} , L_{reg} and L_{mask} to FCOS and Condinst. All of three losses are calculated and averaged over all locations associated with arbitrary ground truth instance.

Training Implementation. We follow the training implementation of Condinst [41]. The model adopts Resnet-50, Resnet-101 [14] with FPN [21] as backbones. Weights in the backbone are initialized with ImageNet pre-trained weights. Weights in other layers are initialized as in [22]. The model is trained with SGD over 8 A100 GPUs for 90K iterations. Hyperparameter setting: Initial learning rate 0.01, mini-batch size 16, weight decay 0.0001, momentum 0.9. The learning rate decays by the factor of 0.1 at iteration 60K and 80K. At the beginning of the training, a 1000-iteration warmup with fixed linear learning rate decay is performed. The warmup factor is 0.001. Maintaining the aspect ratio, the input images are resized to have the longer side less equal to 1333 and shorter side in [640, 800] during training. Left-right flipping data augmentation is also adopted in the training.

Inference. Given the tap query on the image, TraceNet first aligns the tap to the five nearest location at each feature map, one per feature map. Then RFT backtraces recursively all the receptive field

regions across all layers with respect to these five locations, such that all the calculation outside the receptive field region does not contribute to the final predicted features at these five locations. AutoCropping and Autopadding are performed during the forwarding pass. The forwarding pass predicts $5 \times C$ candidate foreground bounding boxes/parameter vectors associated with the instance in total, where C indicates the category class of the dataset. NMS on bounding box with threshold 0.6 is performed to select the top-1 result for producing the instance mask at the tap.

4 EXPERIMENTS

Table 1: mIoU-T and mTA on LVIS, mTA on COCO. TraceNet highlights our method.

Method	mIoU-T	mTA(LVIS)	mTA(COCO)
ritm-h32 [40]	0.328	0.238	0.349
focuscut-R-50 [24]	0.253	0.0734	0.117
focuscut-R-101 [24]	0.228	0.0744	0.138
TraceNet-R-50-FPN	0.286	0.272	0.346
TraceNet-R-101-FPN	0.294	0.257	0.395

4.1 Evaluation Formulation

Denote a set of ground-truth masks $\{M_{gt}^i\}$, where M_{gt}^i is the ground-truth mask of the i -th instance in the dataset. Denote a set of taps $\{c^{i,j}\}$ where each element $c^{i,j}$ is the j -th tap, $c^{i,j} \in M_{gt}^i$. Denote a set of predicted masks as $\{M_{pred}^{i,j}\}$, where $M_{pred}^{i,j}$ is the predicted mask of the i -th instance when being queried by $c^{i,j}$.

4.2 Evaluation Protocol

We propose two metrics for tap-driven segmentation task, mean Tap Intersection over Union (mIoU-T) and mean Tap Area (mTA) as discussed in Section 3.

Mean Tap Intersection Over Union. Since the predicted mask M_{pred} depends on the user tap, IoU cannot be directly applied to measure the expectation of mask quality with different user taps. We propose mIoU-T that measures the average quality of a set of predicted masks $\{M_{pred}^{i,j}\}$ over a set of instances with ground-truth mask M_{gt}^i .

$$mIoU_T = \frac{\sum_{i,j} \text{Area}(M_{pred}^{i,j} \cap M_{gt}^i)}{\sum_{i,j} \text{Area}(M_{pred}^{i,j} \cup M_{gt}^i)} \quad (6)$$

This is a general metric that works on arbitrary numbers of one-shot tap queries and arbitrary numbers of instances. In our experiment, the number of taps is a constant within each instance, i.e for any $i, j \in [k]$, where k is a constant value indicating the size of the set of candidate one-shot tap queries for an instance.

Mean Tap Area. Besides the expectation of predicted mask quality, the user tap tolerance is measured, i.e., the proportion of the region that a user tap can fall into for a high-quality single-instance mask. We propose to use mTA to measure user tap tolerance. To calculate

Table 2: mIoU-T over categories on COCO dataset.

Method	person	car	chair	bottle	cup	dining table	traffic light	bowl	Category Total
mobilesam [49]	0.4877	0.5129	0.3530	0.6043	0.6405	0.2571	0.3425	0.3675	0.4331
focuscut-R-50 [24]	0.4128	0.3734	0.3703	0.3705	0.4715	0.2206	0.3652	0.4631	0.3774
focuscut-R-101 [24]	0.4759	0.4150	0.3961	0.3079	0.3610	0.2735	0.3122	0.4411	0.4217
TraceNet-R-50-FPN	0.4306	0.4796	0.3285	0.090	0.1631	0.5010	0.2925	0.2541	0.3977
TraceNet-R-101-FPN	0.4542	0.5186	0.3787	0.0958	0.1798	0.5207	0.4471	0.2733	0.4312

Table 3: Computation Cost to Retrieve an Instance from an image of size of 1024 x 768. TraceNet highlights our method. FullNet refers to our model without RFT.

Method	throughput	latency (ms)	FLOPs
mobilesam [49]	40.81	24.50	-
ritm-h32 [40]	11.37	87.94	406.5G
focuscut-R-50 [24]	44.33	22.56	52.55G
focuscut-R-101 [24]	37.86	26.42	67.18G
FullNet-R-50-FPN	-	-	86.67G
FullNet-R-101-FPN	-	-	118.28G
TraceNet-R-50-FPN	48.85	20.47	34.47G
TraceNet-R-101-FPN	41.96	23.83	66.67G

the feasible region of user tap, for any i , $\{c^{i,j}\}$ should be constructed as a set of all pixels in the M_{gt}^i . mTA is calculated as below:

$$mTA = \frac{\sum_{i,j} \mathbb{1}(\text{IoU}(M_{\text{pred}}^{i,j}, M_{\text{gt}}^i) \geq \beta)}{\sum_i \text{Area}(M_{\text{gt}}^i)} \quad (7)$$

where β is a pre-defined IoU threshold and $\mathbb{1}$ is an indicator function. We use Eq. 4.2 rather than averaging among each of the trials to treat instances of various sizes equally.

4.3 Implementation Detail

Dataset We train and evaluate TraceNet on MS-COCO [23] and LVIS [12]. MS-COCO is a large-scale dataset for object detection and instance segmentation with over 82k training images and 600k instance-level mask annotations. LVIS is a dataset built from the images in MS-COCO for large vocabulary instance segmentation. It has 2-million high-quality instance mask annotations over 1k entry-level categories.

Tap Simulation with Morphological Transformations. Since no taps are provided in the dataset, we have to simulate user taps within all instances in the dataset. During evaluation, 25 user taps $\{c^{i,j}\}$ are simulated within all instances in the dataset. We sample 25 taps for one instance, with each five taps randomly sampled in one of the five bands around the moment of the instance. The boundary between bands is constructed with the help of morphological transformations, as is described as follows: Suppose the instance is bounded by a bounding box in $H \times W$. Then we construct an binary image $I \in \{0, 1\}^{H \times W}$, where only the pixel value at moment of the instance is one. The first boundary between bands is generated by performing dilation on the I with kernel size $H/5 \times W/5$. More boundaries are generated by performing the same dilation

operation repeatedly. The generated taps are visualized in the Figure 4.

4.4 Quantitative Evaluation

Baselines. ritm [40] is a computationally heavy click-based interactive segmentation model with the strongest one-click performance before SAM [19]. focuscut [24] is a state-of-the-art efficient click-based interactive segmentation model with the ResNet backbone. For a fair comparison, focuscut, ritm, and our models are trained on LVIS + COCO. Mobilesam is trained on a significantly larger dataset proposed in the SAM paper.

mIoU-T. We evaluate the overall IoU-T performance of our method on COCO and LVIS. As shown in Table 1 and Table 2, the TraceNet with ResNet backbone outperforms focuscut with the same backbone. The performance is slightly lower than heavy ritm and mobilesam with more training data. In the category analysis, our model achieves good performance on common and large object categories (e.g. dining table and car) but loses performance in small ones (e.g. bottle and cup) compared to baselines. The intuition is that global features eliminated by RFT module are important when extracting segmentation masks of relatively small objects. However, the property of performing better in large salient objects than small objects are favoured in mobile applications, since people intend to zoom in to click on the instance in real-time editing or capturing.

mTA. mTAs of TraceNet on COCO are 0.346 and 0.395 with ResNet-50 and RestNet-101 backbone, respectively. It indicates that over 30% of the user taps can result in a good instance mask with IoU larger than 0.7. A significant drop in terms of mTA is observed on LVIS. Since the LVIS dataset provides more fine-grained annotations of the image in COCO. Overall, TraceNet achieves significantly better mTA than baselines, demonstrating robustness to tap locations.

Performance Profiling over Band The mIoU-T and mTA performance over 5 different bands are profiled in Figure 5. As it is shown in the figure, both mIoU-T and mTA drop with the distance to the instance center. As it is shown in the second row of Figure 5, a good instance mask could be obtained within the Band-1 and Band-2. The quality of the instance mask will drop significantly when a user tap to a region is far from the instance center.

Computation analysis. Efficiency is one of the most important objectives of one-tap segmentation task for mobile devices. In Table 3, we make an analysis on FLOPs, throughput in one second, and latency of the inference process of the algorithm. With the help of RFT, TraceNet saves 60.2% of computations on R-50-FPN Backbone and 43.6% of computations on R-101-FPN, compared to the full inference process which is denoted as FullNet (for **ablation**).



Figure 4: Generated tap regions from band-1 (left most) to band-5 (right most).

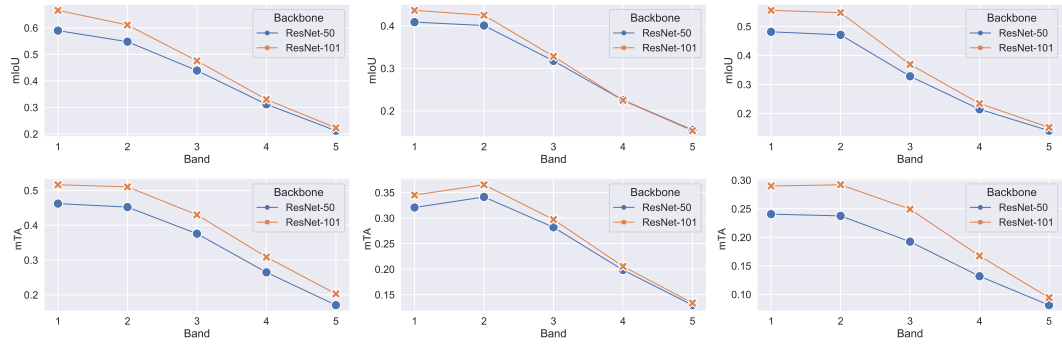


Figure 5: mIoU-T and mTA over different band regions in COCO, LVIS and BDD100K (additional) from left to right



Figure 6: Qualitative Results: first column as groundtruth.

Table 4: Computation Cost of other non-efficient baselines in FLOPs.

Model_backbone	Size of Input	FLOPs
Iseg_SwinB [27]	400 x 400	138.21
Iseg_SwinL [27]	400 x 400	302.78
FocalClick_SegFB3 [9]	256 x 256	24.75
CDNet_R-34 [8]	384 x 384	113.60
SimpleClick_ViT-Tiny [26]	224 x 224	2.63
SimpleClick_ViT-Tiny [26]	448 x 448	10.52
SimpleClick_ViT-H [26]	224 x 224	532.87
SimpleClick_ViT-H [26]	448 x 448	1401.93

TraceNet significantly outperforms all baselines in terms of computation efficiency. To show efficiency superiority of Tracenet, we also include table 4 showing extremely high flops of non-efficient interactive segmentation algorithms on input images of much smaller resolution. Most of them are transformer based models. The FLOPs of a transformer block scales quickly with increase in input resolution. It can be calculated as $12nd^2 + 2n^2d$. [36]. n denotes the input

sequence length and d denotes the embedding dimension. Large Model such as SAM is even more expensive than the above mentioned models and takes 0.15s per frame on Nvidia A100 GPU. In terms of memory consumption, TraceNet, with its minimal requirement of only 12.5M parameters for inference, is optimally designed to meet the demands of mobile devices.

4.5 Qualitative Result Evaluation

The qualitative evaluation of our TraceNet method is depicted in Figure 6. In the first column of each image set, we present the comprehensive ground-truth segmentation masks that encompass all dataset categories represented within each single image. The subsequent columns showcase the results of instance masks generated from user interactions, where users have performed a random tap, selecting one instance at a time. The displayed results demonstrate the exceptional performance of the TraceNet in producing instance masks. Remarkably, the model requires only a single user tap per instance to predict the masks with high precision. This level of accuracy is mostly maintained even when the tap is placed on the non-centered regions of an instance. This robustness of TraceNet demonstrates the model's excellent ability to segment the full extent of an instance from minimal and potentially suboptimal input. Such capabilities are indicative of model's advances understanding of the contextual information at all levels within the images, making it an ideal candidate for camera applications that benefit from on-the-fly photo editing features, where users may prefer quick and intuitive interactions with the editing tool.

5 CONCLUSION

In this paper, we propose and formulate one-tap efficient segmentation task. We also design the evaluation protocol including mIoU-T and mTA metrics. We build our solution TraceNet that back-traces the receptive field region at each layer with respect to local features around the user query tap. TraceNet demonstrates effectiveness and efficiency in the inference process, potentially benefiting on-the-fly mobile image editing applications. TraceNet serves as a practical efficient and interactive solution on mobile before we achieve extremely fast inference of large promptable models. Besides, the success of TraceNet shows potentials to leverage one "referring" modality to significantly increase efficiency.

REFERENCES

- [1] Amazon. 2023. *Amazon Flows*. <https://www.amazon.com/A9-Innovations-LLC-Powered-Amazon/dp/B008G318PE>
- [2] André Araujo, Wade Norris, and Jack Sim. 2019. Computing Receptive Fields of Convolutional Neural Networks. *Distill* (2019). <https://doi.org/10.23915/distill.00021> <https://distill.pub/2019/computing-receptive-fields>.
- [3] Daniel Bolya, Chong Zhou, Fanyi Xiao, and Yong Jae Lee. 2020. YOLACT++: Better Real-time Instance Segmentation. *IEEE Transactions on Pattern Analysis and Machine Intelligence* (2020).
- [4] Daniel Bolya, Chong Zhou, Fanyi Xiao, and Yong Jae Lee. 2020. YOLACT++: Better Real-time Instance Segmentation. *IEEE Transactions on Pattern Analysis and Machine Intelligence* (2020).
- [5] Y.Y. Boykov and M.-P. Jolly. 2001. Interactive graph cuts for optimal boundary & region segmentation of objects in N-D images. In *Proceedings Eighth IEEE International Conference on Computer Vision. ICCV 2001*, Vol. 1. 105–112 vol.1. <https://doi.org/10.1109/ICCV.2001.937505>
- [6] Jiale Cao, Rao Muhammad Anwer, Hisham Cholakkal, Fahad Shahbaz Khan, Yanwei Pang, and Ling Shao. 2020. SipMask: Spatial Information Preservation for Fast Image and Video Instance Segmentation. *Proc. European Conference on Computer Vision* (2020).
- [7] Liang-Chieh Chen, Yukun Zhu, George Papandreou, Florian Schroff, and Hartwig Adam. 2018. Encoder-Decoder with Atrous Separable Convolution for Semantic Image Segmentation. In *ECCV*.
- [8] Xi Chen, Zhiyan Zhao, Feiwei Yu, Yilei Zhang, and Manni Duan. 2021. Conditional Diffusion for Interactive Segmentation. In *2021 IEEE/CVF International Conference on Computer Vision (ICCV)*. 7325–7334. <https://doi.org/10.1109/ICCV48922.2021.00725>
- [9] Xi Chen, Zhiyan Zhao, Yilei Zhang, Manni Duan, Donglian Qi, and Hengshuang Zhao. 2022. FocalClick: Towards Practical Interactive Image Segmentation. In *IEEE/CVF Conference on Computer Vision and Pattern Recognition, CVPR 2022, New Orleans, LA, USA, June 18–24, 2022*. IEEE, 1290–1299. <https://doi.org/10.1109/CVPR52688.2022.00136>
- [10] Bowen Cheng, Ishan Misra, Alexander G. Schwing, Alexander Kirillov, and Rohit Girdhar. 2022. Masked-attention Mask Transformer for Universal Image Segmentation. *CVPR*.
- [11] L. Grady. 2006. Random Walks for Image Segmentation. *IEEE Transactions on Pattern Analysis and Machine Intelligence* 28, 11 (2006), 1768–1783. <https://doi.org/10.1109/TPAMI.2006.233>
- [12] Agrim Gupta, Piotr Dollár, and Ross Girshick. 2019. LvIs: A dataset for large vocabulary instance segmentation. In *Proceedings of the IEEE/CVF conference on computer vision and pattern recognition*. 5356–5364.
- [13] Kaiming He, Georgia Gkioxari, Piotr Dollár, and Ross Girshick. 2017. Mask R-CNN. In *2017 IEEE International Conference on Computer Vision (ICCV)*. 2980–2988. <https://doi.org/10.1109/ICCV.2017.322>
- [14] Kaiming He, X. Zhang, Shaoqing Ren, and Jian Sun. 2016. Deep Residual Learning for Image Recognition. *2016 IEEE Conference on Computer Vision and Pattern Recognition (CVPR)* (2016), 770–778.
- [15] Andrew Howard, Mark Sandler, Grace Chu, Liang-Chieh Chen, Bo Chen, Mingxing Tan, Weijun Wang, Yukun Zhu, Ruoming Pang, Vijay Vasudevan, Quoc V. Le, and Hartwig Adam. 2019. Searching for MobileNetV3. In *ICCV*.
- [16] Jie Hu, Liujuan Cao, Yao Lu, ShengChuan Zhang, Yan Wang, Ke Li, Feiyue Huang, Ling Shao, and Rongrong Ji. 2021. Istr: End-to-end instance segmentation with transformers. *arXiv preprint arXiv:2105.00637* (2021).
- [17] Sergey Ioffe and Christian Szegedy. 2015. Batch Normalization: Accelerating Deep Network Training by Reducing Internal Covariate Shift. In *Proceedings of the 32nd International Conference on Machine Learning (Proceedings of Machine Learning Research, Vol. 37)*, Francis Bach and David Blei (Eds.). PMLR, Lille, France, 448–456. <https://proceedings.mlr.press/v37/ioffe15.html>
- [18] Won-Dong Jang and Chang-Su Kim. 2019. Interactive Image Segmentation via Backpropagating Refinement Scheme. In *Proceedings of The IEEE Conference on Computer Vision and Pattern Recognition*.
- [19] Alexander Kirillov, Eric Mintun, Nikhila Ravi, Hanzi Mao, Chloe Rolland, Laura Gustafson, Tete Xiao, Spencer Whitehead, Alexander C. Berg, Wan-Yen Lo, Piotr Dollár, and Ross B. Girshick. 2023. Segment Anything. *2023 IEEE/CVF International Conference on Computer Vision (ICCV)* (2023), 3992–4003. <https://api.semanticscholar.org/CorpusID:257952310>
- [20] Youngwan Lee and Jongyoul Park. 2020. CenterMask: Real-Time Anchor-Free Instance Segmentation. (2020).
- [21] Tsung-Yi Lin, Piotr Dollár, Ross Girshick, Kaiming He, Bharath Hariharan, and Serge Belongie. 2017. Feature Pyramid Networks for Object Detection. In *2017 IEEE Conference on Computer Vision and Pattern Recognition (CVPR)*. 936–944. <https://doi.org/10.1109/CVPR.2017.106>
- [22] Tsung-Yi Lin, Priya Goyal, Ross B. Girshick, Kaiming He, and Piotr Dollár. 2017. Focal Loss for Dense Object Detection. *2017 IEEE International Conference on Computer Vision (ICCV)* (2017), 2999–3007.
- [23] Tsung-Yi Lin, Michael Maire, Serge Belongie, James Hays, Pietro Perona, Deva Ramanan, Piotr Dollár, and C Lawrence Zitnick. 2014. Microsoft coco: Common

objects in context. In *European conference on computer vision*. Springer, 740–755.

[24] Zheng Lin, Zheng-Peng Duan, Zhao Zhang, Chun-Le Guo, and Ming-Ming Cheng. 2022. FocusCut: Diving into a Focus View in Interactive Segmentation. In *2022 IEEE/CVF Conference on Computer Vision and Pattern Recognition (CVPR)*. 2627–2636. <https://doi.org/10.1109/CVPR52688.2022.00266>

[25] Zheng Lin, Zhao Zhang, Lin-Zhuo Chen, Ming-Ming Cheng, and Shao-Ping Lu. 2020. Interactive Image Segmentation With First Click Attention. In *2020 IEEE/CVF Conference on Computer Vision and Pattern Recognition (CVPR)*. 13336–13345. <https://doi.org/10.1109/CVPR42600.2020.01335>

[26] Qin Liu, Zhenlin Xu, Gedas Bertasius, and Marc Niethammer. 2023. SimpleClick: Interactive Image Segmentation with Simple Vision Transformers. *arXiv:2210.11006 [cs.CV]*

[27] Qin Liu, Zhenlin Xu, Yining Jiao, and Marc Niethammer. 2022. ISegFormer: Interactive Segmentation Via Transformers With Application To 3D Knee MR Images. In *Medical Image Computing and Computer Assisted Intervention – MICCAI 2022: 25th International Conference, Singapore, September 18–22, 2022, Proceedings, Part V* (Singapore, Singapore). Springer-Verlag, Berlin, Heidelberg, 464–474. https://doi.org/10.1007/978-3-031-16443-9_45

[28] Qin Liu, Meng Zheng, Benjamin Planche, Srikrishna Karanam, Terrence Chen, Marc Niethammer, and Ziyan Wu. 2022. PseudoClick: Interactive Image Segmentation with Click Imitation. <https://doi.org/10.48550/ARXIV.2207.05282>

[29] Google LLC. 2023. *Google Lens*. <https://blog.google/products/google-lens/google-lens-features/>

[30] Jonathan Long, Evan Shelhamer, and Trevor Darrell. 2015. Fully convolutional networks for semantic segmentation. In *2015 IEEE Conference on Computer Vision and Pattern Recognition (CVPR)*. 3431–3440. <https://doi.org/10.1109/CVPR.2015.7298965>

[31] Wenjie Luo, Yujia Li, Raquel Urtasun, and Richard Zemel. 2016. Understanding the Effective Receptive Field in Deep Convolutional Neural Networks. In *Proceedings of the 30th International Conference on Neural Information Processing Systems* (Barcelona, Spain) (NIPS’16). Curran Associates Inc., Red Hook, NY, USA, 4905–4913.

[32] Microsoft. 2020. *Microsoft Seeing AI*. <https://www.microsoft.com/en-us/garage/wall-of-fame/seeing-ai/>

[33] Eric N. Mortensen and William A. Barrett. 1995. Intelligent Scissors for Image Composition. In *Proceedings of the 22nd Annual Conference on Computer Graphics and Interactive Techniques (SIGGRAPH ’95)*. Association for Computing Machinery, New York, NY, USA, 191–198. <https://doi.org/10.1145/218380.218442>

[34] Eric N. Mortensen and William A. Barrett. 1998. Interactive Segmentation with Intelligent Scissors. *Graph Models Image Process.* 60, 5 (sep 1998), 349–384. <https://doi.org/10.1006/gmip.1998.0480>

[35] Mahyar Najibi, Bharat Singh, and Larry S Davis. 2019. AutoFocus: Efficient Multi-Scale Inference. *ICCV* (2019).

[36] Zizheng Pan, Bohan Zhuang, Jing Liu, Haoyu He, and Jianfei Cai. 2021. Scalable Vision Transformers With Hierarchical Pooling. In *Proceedings of the IEEE/CVF International Conference on Computer Vision (ICCV)*. 377–386.

[37] Carsten Rother, Vladimir Kolmogorov, and Andrew Blake. 2004. "GrabCut": Interactive Foreground Extraction Using Iterated Graph Cuts. *ACM Trans. Graph.* 23, 3 (aug 2004), 309–314. <https://doi.org/10.1145/1015706.1015720>

[38] Mark Sandler, Andrew Howard, Menglong Zhu, Andrey Zhmoginov, and Liang-Chieh Chen. 2018. MobileNetV2: Inverted Residuals and Linear Bottlenecks. In *CVPR*.

[39] Konstantin Sofiiuk, Ilia Petrov, Olga Barinova, and Anton Konushin. 2020. f-brs: Rethinking backpropagating refinement for interactive segmentation. In *Proceedings of the IEEE/CVF Conference on Computer Vision and Pattern Recognition*. 8623–8632.

[40] Konstantin Sofiiuk, Ilya A. Petrov, and Anton Konushin. 2022. Reviving Iterative Training with Mask Guidance for Interactive Segmentation. In *2022 IEEE International Conference on Image Processing (ICIP)*. 3141–3145. <https://doi.org/10.1109/ICIP46576.2022.9897365>

[41] Zhi Tian, Chunhua Shen, and Hao Chen. 2020. Conditional Convolutions for Instance Segmentation. In *Proc. Eur. Conf. Computer Vision (ECCV)*.

[42] Zhi Tian, Chunhua Shen, Hao Chen, and Tong He. 2021. FCOS: A Simple and Strong Anchor-free Object Detector. (2021).

[43] Zhi Tian, Bowen Zhang, Hao Chen, and Chunhua Shen. 2022. Instance and Panoptic Segmentation Using Conditional Convolutions. *IEEE Transactions on Pattern Analysis and Machine Intelligence* (2022), 1–1. <https://doi.org/10.1109/TPAMI.2022.3145407>

[44] Xinlong Wang, Rufeng Zhang, Tao Kong, Lei Li, and Chunhua Shen. 2020. SOLOv2: Dynamic and Fast Instance Segmentation. *Proc. Advances in Neural Information Processing Systems (NeurIPS)* (2020).

[45] Enze Xie, Peize Sun, Xiaoge Song, Wenhui Wang, Xuebo Liu, Ding Liang, Chunhua Shen, and Ping Luo. 2019. PolarMask: Single Shot Instance Segmentation with Polar Representation. *arXiv preprint arXiv:1909.13226* (2019).

[46] Ning Xu, Brian L. Price, Scott Cohen, Jimei Yang, and Thomas S. Huang. 2016. Deep Interactive Object Selection. In *2016 IEEE Conference on Computer Vision and Pattern Recognition, CVPR 2016, Las Vegas, NV, USA, June 27–30, 2016*. IEEE Computer Society, 373–381. <https://doi.org/10.1109/CVPR.2016.47>

[47] Chenhongyi Yang, Zehao Huang, and Naiyan Wang. 2021. QueryDet: Cascaded Sparse Query for Accelerating High-Resolution Small Object Detection. *arXiv preprint arXiv:2103.09136* (2021).

[48] Xiaodong Yu, Dahu Shi, Xing Wei, Ye Ren, Tingqun Ye, and Wenming Tan. 2022. SOIT: Segmenting Objects with Instance-Aware Transformers. In *Proceedings of the AAAI Conference on Artificial Intelligence*. 3188–3196.

[49] Chaoning Zhang, Dongshen Han, Yu Qiao, Jung Uk Kim, Sung-Ho Bae, Seungkyu Lee, and Choong Seon Hong. 2023. Faster Segment Anything: Towards Light-weight SAM for Mobile Applications. *arXiv preprint arXiv:2306.14289* (2023).

[50] Minghao Zhou, Hong Wang, Qian Zhao, Yuexiang Li, Yawen Huang, Deyu Meng, and Yefeng Zheng. 2023. Interactive Segmentation as Gaussian Process Classification. *arXiv:2302.14578 [cs.CV]*

[51] Xueyan Zou, Jianwei Yang, Hao Zhang, Feng Li, Linjie Li, Jianfeng Wang, Lijuan Wang, Jianfeng Gao, and Yong Jae Lee. 2023. Segment Everything Everywhere All at Once. In *Thirty-seventh Conference on Neural Information Processing Systems*. <https://openreview.net/forum?id=UHBrWeFWl>